DFT Functional Analysis for the Modeling Raman Bands and Absorption Spectra of the Lycopene Structure

Mindaugas Macernis

Institute of Chemical physics, Faculty of Physics, Vilnius University, Saulėtekio al. Vilnius, Lithuania

Corresponding Author: *Mindaugas Macernis, Institute of Chemical physics, Faculty of Physics, Vilnius University, Saulėtekio al. Vilnius, Lithuania, mindaugas.macernis@ff.vu.lt*

ABSTRACT

The different length carotenoids have linear correlation between the Raman v1band and S0-S2 absorption. The possible distortions in carotenoids due to dimer effects may change the correlation what can be modelled by using DFT methods. Thus, DFT functional must be suitable to predict good geometries, Raman and UV absorption (S0-S2) spectra. This should be true for the monomer and dimer structures.It is known that not all DFT functional are suitable for all this type calculation. We performed DFT functional analyses on the lycopene which represents typical carotenoid molecule. We have analyzed 281 different DFT functional. The analysis was based on the 4 type calculations: monomer geometry optimization, monomer Raman spectra, monomer excited states and H-dimerexcited state splitting at different distances. According results there wasn't one particular functional which could be suitable for the all 4 different type calculations. In the paper we classified DFT functional which are the best for the geometry optimization, monomer Raman, monomerexited states and H-dimerexcited state splitting calculations.

Keywords: *TD-DFT; Raman;DFT; lycopene; carotenoids*

INTRODUCTION

Raman spectroscopic together with absorption spectra techniques are a group of chemical fingerprint detection methods based on molecular vibrational spectroscopy[1-3]. They are used for various applications as well as for Carotenoids (Cars) study [1-10].

The portable Raman spectroscopicinstruments could be used to monitor the health and safety compliance of herbal products in the consumer market [1]. The Raman spectroscopy can be used in various aspects of mycobacterial physiology, e.g. it describes a novel effect of carbon source variation on mycobacteria [2]. The presence of Cars in the amoeba is observed via characteristic Raman bands [4]. Resonance Raman indicates that Carchromophore must be in an all-*trans* configuration in Orange carotenoid protein [3]. Using recorded Raman spectra Cars in copper-sulfates could be used as biomarkers what is useful proxies for understanding remote mineral formations as well as for terrestrial environmental investigations and biological activity [5]. Resonance Raman spectroscopy is used to evaluate the structure of light-harvesting chlorophyll a/b complexes of photosystem II, reconstituted from wild-type and mutant apoproteins over-expressed in

Escherichia coli [7]. In ref. [6] a selection of applications is presented, in order to illustrate how Resonance Raman spectroscopy techniques have been used in the field of photosynthesis, and what type of information has been obtained.

Cars are important actors both in light-harvesting and in photo protection functions of photosynthetic pigment–protein complexes.

A systematic change in the Raman line widths in the ground state can be satisfactorily explained as a function of the viscosity of the surrounding media. Even when the absorption peaks appear at the same energy, the vibrational decay time of spheroidene in the Light-Harvesting Complex II is approximately 15–20% slower than that in organic solvents [8].

The electrochemical properties of the compounds is strongly influenced by the functional groups on the unsaturated phytyl chains (carboxylic acid, alcohol, ester, or aldehyde groups), and not only on the fully conjugated hydrocarbon unit which is common to all forms of vitamin A [9].

However, a deep theoretical investigation of this multiple role related to Cars is still missing owing to the difficulty of describing the delicate interplay between electronic and nuclear degrees of freedom in calculations [10].

It is possible to distinguish different Cars by the position of their v_1 Raman mode and the absorption spectra (related to their excitation profile). Analysis of the v_4 Raman band indicates that theCars are present in a specific consistent with their binding to specific proteins [11]. The symmetry breaking in Cars with nonlinear π-electron system (e.g. *cis-β*-carotenes) is of virtually no effect on the dark transitions in these pigments [12]. However the *cis-trans* isomerization should be important for other chemical and biological functions [13-16]. It is known the light-induced *cis-trans* isomerization of prolycopene to all-*trans*-lycopene (LYC) occurs through the triplet states [13]. Moreover,the LYC is present in its all-*trans* isomeric from in vegetables and fruits, while cis-isomers constitute the predominant form present in the serum and tissues [14-16].

The LYC is typical Car from the ripe fruit of tomato which is widely investigated [14-16].

The absorption spectrum of Cars depends on the length of the conjugated chain and it is sensitive solvent properties [17-22]. The absorption bands correspond to a S_0–S_2 electronic transition in the visible spectral range [23].The lowest S_1 (or $1^1A_g^-$) state is predicted almost 50 years ago[23-25]and it is absorption-silent. Cars must have morelow-energy excited statesaccording analysis of the time-resolved experiments [24, 26-30]. All of the different roles of Cars rely on the electronic properties of their linear, conjugated polyene chain. These characteristics give the Car molecule its absorption properties, most often in the blue-green range, which correspond to an electronic transition from the ground (S_0) to the second (S_2) electronic state. A direct relationship between the S_0–S_2 absorption band and the length of the conjugated chain has been established early [31-35]. However, the whole electronic structure of Cars molecules turns out to be extremely complex.

The Resonance Raman, as a vibrational technique, is among the best methods to characterize the structural and electronic properties of Car molecules. Resonance Raman scattering occurs when the wavelength of the laser's excitation is in close proximity to an intense electronic absorption band.

The Resonance Raman signal intensities may display enhancement up to six orders of magnitude as compared to normal Raman scattering [36], which is the case for Cars. Resonance Raman spectra of Cars contain three main bands indicated as v_1, v_2, v_3 and in some cases v_4 [37]. The $v_1$arises from the stretching modes of the C=C bonds.The v_2 band arises from a combination of C-C stretching modes and in-plane C-C bending modes. The v_3 bandarises from the coupling of the in-plane rocking vibrations of the methyl groups attached to the conjugation chain, with the adjacent C-H in-plane bending. A weak v_4 band arises from C-H out-of-plane wagging motions coupled with C=C torsional modes.The frequency of the Raman v_1 bandcan be considered as a direct measure of the conjugation length of the chain [38]what is important in order understand excited state dynamics.The Raman v_1 of Cars represents C=C stretching modes of carotenoids [37] andit gives access to the structure of the conjugated double bond chain.

Resonance Raman spectroscopy has proven to be a very sensitive and useful technique for various Car studies, but would gain larger precision if the spectral variations observed in biology could be more finely interpreted. Despite the apparent simplicity of Cars structure, calculating the electronic and vibrational properties of Cars with reasonable precision has only recently become possible through the application of DFT and TD-DFT [37,39,40].It is known Cars with the different length have linear correlation between Raman v_1 band and S_0-S_2 absorption which can be modelled [37]. However it is not clear which DFT functional are suitable for all types modelling of Cars including monomer and dimer structures.The aim of our study was to investigate the DFT functional in order to classify which functional were the best suitable for the calculation of the monomer S_2 excited state ($1^1B_u^+$), dimer S_2 excited state ($1^1B_u^+$) and monomer Raman v_1, v_2, v_3 bands according the well-known LYC carotenoid experimental data [37, 41].

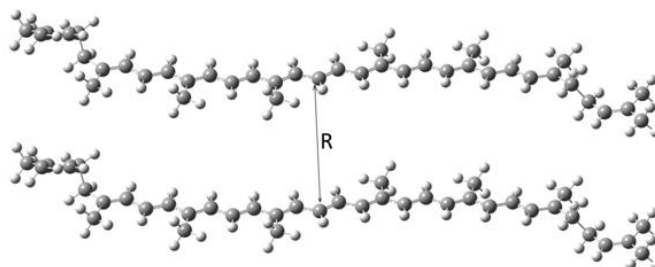## CALCULATIONS AND INVESTIGATED STRUCTURES

Calculation Details

The calculations were performed using the Gaussian 09 program package (Rev D.01) [42]. The LYC structures where computed using DFT theory with chosen functional and 6-311G(d,p) basis set. All LYC structures were modeled in the gas phase (vacuum). Additionally, the LYC molecules using different DFT functional were characterized by frequency analysis where frequency calculations having all real frequencies

identify minimum structures. We performed calculationswith 281 DFT functionalfor monomer excited states, *H*-dimer excited states and monomer Raman of LYC. The majority of the DFT functional had various problems. Thus they weren't listed in the paper. Contact the corresponding author for the full list.

Lycopene Structure and Its UV, Raman Spectra

Lycopene ($C_{40}H_{56}$) consists of eight isoprenic units and its conjugation length N is 11 (Fig. 1).

LYC structure according cis and *trans* of double bonds can be made into 72 different isomers forms [43]. Moreover the structure can have 1056 theoretical *cis-trans* configurations [43]. The LYC structure can be found in the PDB bank as 1LGH [44] where the structure is all-*trans* type (see Fig 1 A). Sometimes all-*trans*LYC are labeled as *E*-isomer while *cis* structures of LYC are labeled as *Z*-isomer (e.g. 5-cis would beZ5-isomer).The all-trans-lycopene (LYC) structure will be used for DFT functional analysis in this paper.

**Fig1.** *H-dimer of Lycopene structure. R – Distance between structures.*

The lowest electronic excited states of LYC(as it is true for all Cars) are mainly defined by the excited states of the polyene chain.This leads thatthe transition from the ground state to the first excited state ($2^1A_g^-$) is forbidden due to the symmetry restrictions [24,41,45].

The state has a dominant double excitation character (HOMO2→LUMO2). The optically allowed transition into the second excited state of the $1^1B_u^+$ symmetry is mainly caused by the single excitation character (HOMO→LUMO transition). The excited state of the $1^1B_u^+$ symmetry (corresponding to the S_0–S_2 transition) for the polyenes and Cars can be

predicted in terms of the TD-DFT theory [41, 46] as it is S_0–S_1 transition in calculation data. The $2^1A_g^-$ type excited state can be predicted by TD-DFT using BLYP functional with Tamm-Dancoff approximations because there are errors in both methods only [47]. Between $2^1A_g^-$ and $1^1B_u^+$ type excited state there are other excited states but they cannot be predicted using TD-DFT theories also[41,46,47].

From the TD-DFT calculations the DFT functional predicting the lowest HOMO-LUMO type allowed $1^1B_u^+$ typestate can be classified as suitable for the UV type caculations.
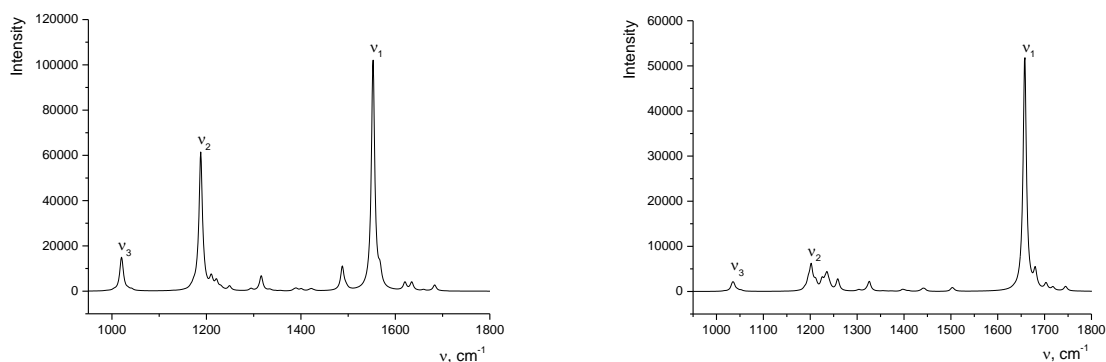
Fig2. *Lycopene Raman spectra of lycopene monomer according different calculation models: A –B3LYP/6-311G(d,p) method; B – CAM-B3LYP/6-311G(d,p) method.*

Resonance Raman spectra of Car contain four main bands termed v_1 to v_4 (Fig. 2).The most intense band, v_1, located around 1500 cm^{-1}, arises from the stretching modes of the C=C

bonds [37]. The v_2 band at 1160 cm^{-1} arises from a combination of C-C stretching modes and in-plane C-C bending modes [48]. The v_3 band at 1000 cm^{-1} arises from the coupling of the in-

plane rocking vibrations of the methyl groups attached to the conjugation chain, with the adjacent C-H in-plane bending. A weak ν_4 band at about 950 cm^{-1} arises from C-H out-of-plane wagging motions coupled with C=C torsional modes. For planar molecules, such as all-*trans*-lycopene, these modes are expected to be unconjugated with the electronic transition, and accordingly this band should be extremely weak. However, it gains intensity when the molecules get distorted around C-C bonds, and is used as a fingerprint of the molecular conformation [49-51].

Thus if the DFT functionalpredicts ν_1, ν_2,ν_3 bands for the Cars (e.g. LYC) than DFT functionalcan be classified as suitable for the Raman type caculations.

H-Dimer Excitonic Effect Calculations

Typically,*H*-dimers have excitonic splitting effect which decreases when the distance is increasing between the structures (as it was in Fig. 3A). *H*-dimer were made artificially and calculated with TD-DFT method (Fig. 1). Before modeling there were done optimization of the LYC monomer geometry with chosen functional and 6-311G(d,p) basis set. The distance was changed from 5 Å to 50 Å. In Fig. 1 the dashed line shows the calculated monomer value. When the distance was very large at 50 Å than the energy difference of the excitonic splitting become very small and the both excitation values are close to monomer excitation value.

The lower state oscillator f values were close to zero what means the states were forbidden.The higher state had nonzero f values what meant the states are allowed. The CAM-B3LYP functional (Fig. 3 A) predicted quite good excitonic splitting effect while B3LYP functional failed to do it (Fig. 3 B). The DFT functional predicting the two lowest splitted states for the *H*-dimer with above described properties could be classified as suitable for the UV type caculations for the *H*-dimer of LYC structures.

If DFT functional predicted excitonic splitting effect in *H*-dimer than itshould be siutable for *J*-dimer and other dimer of Cars also.
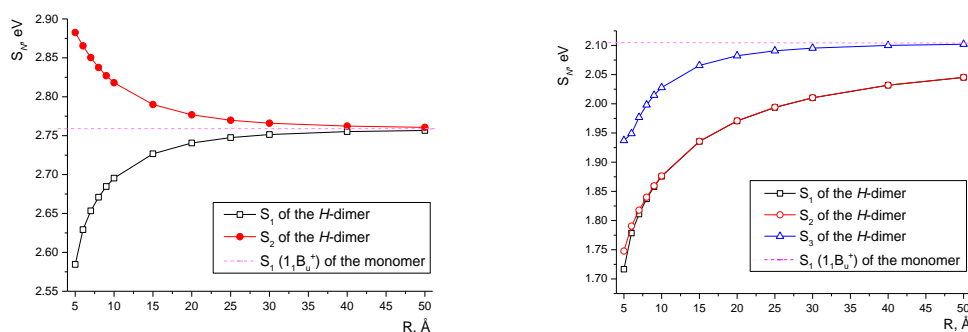
Fig3. *Lycopene absorption spectra for H-dimer according different calculation models: A – CAM-B3LYP/6-311G(d,p) method; B – B3LYP/6-311G(d,p) method.*

Choosing Basis Sets For Functional Calculations

The 6-31G (d,p) basis set with B3LYP functional is good enough to obtain reasonable results [52]. However the scaling factors are required for calculated frequencies and for calculated S_0-S_2 transition energies in order to obtain a satisfactory agreement with experimental data. The frequencies calculations should be scaled by 0.9613 and 0.97for B3LYP/6-31G (d) and B3LYP/6-31G (d,p) methods [37,52].

The S_0-S_2 transition energies should be scaled by 1.22 for B3LYP/6-31G(d,p)method [37]. The scaling factor is important for comparing calculated and experimental data.

The scaling factors were not used in this paper because this wasn't the primary focus of the work.

In order to show good and bad scenario for LYC monomer and *H*-dimerwe chose B3LYP and CAM-B3LYP functional with 4 different basis sets (Table I).UV spectra calculations were done for the *H*-dimer with *R*=5 Å,*R*=10 Å. Raman spectra ν_1, ν_2, $\nu_3$calculations were performed for the monomer. Before every calculation there were made geometry optimizations with chosen basis set. *H*-dimers were made artificially.They were calculated using TD-DFT method. DS1 and DS2 values were calculated according to formula:

$$DS1 = S_{1,mono} - S_{1,h} \qquad (1)$$

$$DS2 = S_{2,h} - S_{1,mono} \qquad (2)$$

where $S_{1,h}$ and $S_{2,h}$ are the first two excited states of the H-dimer, $S_{1,mono}$ is the first excited state of monomer in the calculation results.

In order the $S_{1,h}$ and $S_{2,h}$ represent excitonic effect of the dimer than the DS1 and DS2 must be always positive.

According experimental data the three Raman values ν_1, ν_2, ν_3 for the carotenoids must be the most intensive values in the results around 1500 cm^{-1}, 1200 cm^{-1} and 1000 cm^{-1}.

If the intensity was below 5% according to the most intensive ν_1 value than it was not distinguishable from the spectra: this meant the DFT functional had bad predictions.

The B3LYP functional DS2 results are always negative in calculations with the 6-31G(d), 6-311G(d,p), cc-pVDZ and cc-pVTZ basis sets (Table 1). The CAM-B3LYP functional DS1 and DS2 results were always positive in calculations with the same basis sets.

The Raman intensities I of the ν_1, ν_2, ν_3 were larger than 5% with the B3LYP functional. CAM-B3LYP failed to calculate $I_{\nu3}$ values which were smaller than 5% with all investigated basis sets.

The results showed different basis set didn't make qualitative difference between results while the 6-31G(d) basis set was quite good. In order to have comparative results we chose d6-311G(d,p) basis set for various DFT functional calculations.

Table1. *B3LYP and CAM-B3LYP with different basis set calculations results for H-dimer and Raman of LYC. The good results are those which haven't got negative values or which have Raman intensity about 10%. CAM-B3LYP is good for H-dimer. B3LYP is good for monomer.*

Method	H-dimer, R = 5Å		H-dimer, R = 10Å		Raman of the monomer		
	DS1, eV	DS2, eV	DS1, eV	DS2, eV	$I_{\nu1}$*, %	$I_{\nu2}$, %	$I_{\nu3}$, %
B3LYP/6-31G(d)	0.397	-0.362	0.244	-0.243	100	51.93	9.76
B3LYP/6-311G(d,p)	0.388	-0.357	0.229	-0.228	100	53.85	10.86
B3LYP/cc-pVDZ	0.394	-0.364	0.239	-0.237	100	44.50	7.60
B3LYP/cc-pVTZ	0.388	-0.345	0.224	-0.22	100	56.58	12.27
CAM-B3LYP/6-31G(d)	0.165	0.125	0.063	0.059	100	9.30	3.18
CAM-B3LYP/6-311G(d,p)	0.174	0.124	0.063	0.059	100	8.97	2.16
CAM-B3LYP/cc-pVDZ	0.171	0.125	0.063	0.06	100	5.59	0.03
CAM-B3LYP/cc-pVTZ	0.176	0.123	0.064	0.06	100	9.46	2.17

* - reference intensity (always 100%)

RESULTS

Lycopene Monomer Optimization

The LYC structure optimization using different functional had two major problems. The first problem comes from the fact that the calculation could not be performed with LYC size molecule.

The DFT convergation procedure could not start with 15 DFT functional. The second problem was due to large distortions in the final structure after optimization. The reference structures were the crystallographic data [44] and optimized LYC structure with B3LYP functional.

Firstly, all optimized geometries were checked visually. Then the functional were rejected if there are significant geometrical differences between final and reference structure. The distortion values (bond length, angles between bonds) could not exceed more than 10%

according reference structures. The final calculations reveal 11 DFT functional had very large angles or dihedral angles between heavy atoms. So, all 26 DFT functional were omitted from further analysis in this paper.

TD-DFT Analysis for Lycopene Monomer

TD-DFT calculations should predict the $1^1B_u^+$ state as S_1 and it must have dominating HOMO-LUMO configurations.

The oscillator strength S_1 must be allowed and the S_2 must be forbidden. Thus the other criteria for functional were based on the oscillator strengths for the S_1 and S_2 states.

The S_1 state oscillator strength was chosen to be larger than 0.5 (f>0.5) and S_2 was chosen to be below 0.1 (f<0.1). After calculations the criteria met 92 functional which were suitable for S_1 ($1^1B_u^+$) TD-DFT calculations (Table II).

DFT Functional Analysis for the Modeling Raman Bands and Absorption Spectra of the Lycopene Structure

Table2. *The best DFT functional for $1^1B_u^+$ typestate excitonic splitting according H-dimer and Ramancalculations. The Raman v_1, v_2, v_3 bands intensity value are at least 10% of the largest intensity of the spectra.*

functional suitable for monomer S_1 ($1^1B_u^+$) TD-DFT calculations	functional suitable for *H*-dimer splitting calculations	functional suitable for monomer Raman v_1, v_2, v_3 calculations*	the best functional suitable for monomer Raman v1, v2, v3 calculations
B97D, B97D3, BB95, BBRC, BKCIS, BLYP, BP86, BPBE, BPKZB, BPL, BPW91, BRevTPSS, BRxBRC, BRxPL, BRxVWN, BRxVWN5, BTPSS, BV5LYP, BVP86, BVWN, BVWN5, G96B95, G96BRC, G96KCIS, G96LYP, G96P86, G96PBE, G96PKZB, G96PL, G96PW91, G96RevTPSS, G96TPSS, G96V5LYP, G96VP86, G96VWN, G96VWN5, HCTH, HCTH147, HCTH407, HCTH93, HFB, HFS, M06, mPWB95, mPWBRC, mPWKCIS, mPWLYP, mPWP86, mPWPBE, mPWPKZB, mPWPL, mPWPW91, mPWRevTPSS, mPWTPSS, mPWV5LYP, mPWVP86, mPWVWN, mPWVWN5, N12, OB95, OBRC, OLYP, OP86, OPBE, OPKZB, OPL, OPW91, ORevTPSS, OTPSS, OV5LYP, OVP86, OVWN, OVWN5, PBEB95, PBEBRC, PBEhB95, PBEhBRC, PBEhKCIS, PBEhLYP, PBEhP86, PBEhPBE, PBEhPKZB, PBEhPL, PBEhPW91, PBEhRevTPSS, PBEhTPSS, PBEhV5LYP, PBEhVP86, PBEhVWN, PBEhVWN5, PBEKCIS, PBELYP, PBEP86, PBEPBE, PBEPKZB, PBEPL, PBEPW91, PBERevTPSS, PBETPSS, PBEV5LYP, PBEVP86, PBEVWN, PBEVWN5, PKZBB95, PKZBBRC, PKZBKCIS, PKZBPBE, PKZBPL, PKZBPW91, PKZBRevTPSS, PKZBVWN, PKZBVWN5, PW91B95, PW91BRC, PW91KCIS, PW91LYP, PW91P86, PW91PBE, PW91PKZB, PW91PL, PW91PW91, PW91RevTPSS, PW91TPSS, PW91V5LYP, PW91VP86, PW91VWN, PW91VWN5, RevTPSSBRC, RevTPSSKCIS, RevTPSSPL, RevTPSSVWN, RevTPSSVWN5, SBRC, SKCIS, SLYP, SOGGA11, SP86, SPL, SV5LYP, SVWN, SVWN5, tHCTH, TPSSBRC, TPSSKCIS, TPSSPBE, TPSSPKZB, TPSSPL, TPSSPW91, TPSSRevTPSS, TPSSTPSS, TPSSVWN, TPSSVWN5, wPBEhB95, wPBEhBRC, wPBEhKCIS, wPBEhLYP, wPBEhP86, wPBEhPBE, wPBEhPKZB, wPBEhPL, wPBEhPW91, wPBEhRevTPSS, wPBEhTPSS, wPBEhV5LYP, wPBEhVP86, wPBEhVWN, wPBEhVWN5, XAB95, XAKCIS, XAlpha, XAPBE, XAPL, XAVP86, XAVWN, XAVWN5	BHandH, BHandHLYP, CAM-B3LYP, LC-HCTH, LC-HCTH147, LC-HCTH407, LC-HCTH93, LC-N12, LC-wPBE, M052X, M062X, M06HF, M11, wB97, wB97X, wB97XD	B3LYP, B971, B97D, B97D3, B98, BB95, BBRC, BLYP, BPL, BRxB95, BRxBRC, BRxLYP, BRxPL, BRxVWN, BRxVWN5, BV5LYP, BVWN, BVWN5, HFB, mPWB95, mPWBRC, mPWLYP, mPWPL, mPWV5LYP, mPWVWN, mPWVWN5, N12, OB95, OPL, OVWN, OVWN5, PBEB95, PBEBRC, PBELYP, PBEPL, PBEV5LYP, PBEVWN, PBEVWN5, PW91BRC, PW91LYP, PW91PL, PW91V5LYP, PW91VWN, PW91VWN5	B3LYP, BB95, mPWB95, N12, OB95, PBEB95, PW91BRC

* *Some functional predicts v_4, v_5 at various frequencies (e.g. near v_1) what shouldn't be*

TD-DFT Analysisfor Lycopene H-Dimer

Two LYC molecules put in parallel (*H*-dimer) must have excitonic splitting. The splitting must be larger at the small distance while the splitting must be very small in large distances (as it is in Fig. 3 A). The excitonic splitting analyses were done by artificially making two dimers at 5Å and 10Å distances. If DFT functional results showed excitonic effect than S_1 of the dimer must be below S_1 of the monomer and S_2 of the dimer must be above S_1 of the monomer. The 5Å dimer must be with larger DS1 comparing to DS2 splitting values which was at 10Å dimer(Fig. 3A). Thus DS1 and DS2 must be positive and there must be relations: DS1(R= 5Å) > DS1(R= 10Å); DS2(R= 5Å) > DS2(R= 10Å). According *H*-dimer excitonic effect the dimer S_1 must be forbidden (f<0.1) and the S_2 of the dimer must be allowed (f>0.5). After calculations the 16 DFT functional (Table II) met these criteria and they were suitable for excitonic splitting in *H*-dimer calculations.

Raman Analysis for Lycopene Monomer

Car typical Raman spectra have ν_1, ν_2, ν_3 bands which are around 1500 cm^{-1}, 1150 cm^{-1} and 1000 cm^{-1} respectively. They are clearly seen in Resonance Raman experimental data where intensities are 100%, 94% and 24% for ν_1, ν_2, ν_3 [37,53]. This experimental data wasmajor criteria for Raman spectra [37]. There could be quite good results with the rule 100%, 25%, 5%, where Raman spectra had no more than three bands representing ν_1, ν_2, ν_3 bands: the HSEH1PBE functional met such criteria. However,the rule wasn't good for other functionals because the ν_3 band wouldn't be easy distinguishable from other lines inthe calculated spectra. So there was taken 100%, 50% and 10% criteria which was much closer to experimental data (100%, 94% and 24%) [37,53]. However, the Raman calculations failed to run for the 120 DFT functional due to various reasons (e.g. the functionality wasn't implemented) [42].

The 100%, 50% and 10% criteria for the Raman bands met 44 functional, but there were additional problems. The Raman spectra results with the 20 DFT functional had more than three bands (there must be only 3 intensive Raman bands). The 4 DFT functional had negative values (imaginary frequencies) in frequency calculations. The 13 DFT functional provided some bands which had larger intensity than ν_3 band.

The final calculations result of the suitable functional for the LYC monomer Raman ν_1, ν_2, $\nu_3$bands are shown in Table II.The functional N12 had Raman bands which were about 90% relative intensity of the ν_3 band according to experimental data [37]. Functional B3LYP and PW91BRC had ν_3 Raman bands which were about 80% relatively to experimental data [37]. Functional BB95 had ν_3 Raman bands which are about 70% relatively to experimental data [37]. Finally, functional mPWB95, OB95 and PBEB95 had ν_3 Raman bands which intensities were about 50% relatively to experimental data [37]. So, the B3LYP and N12 functional had the best similarity between calculated and experimental of the whole Raman spectra.

DISCUSSION

The DFT functional analysis show there wasn't one DFTfunctional for LYC which would be suitable to calculate all selected properties. This should be true for all Cars because the LYCmolecule is typical Car. The chosen basis set which was 6-311G(d,p) may be the limitation of calculations. The analysis showed the larger basis set didn't change results significantly. The larger basis set could improve absolute values but it wouldn't overcome functional limitations itself.From results it was clear that all DFT functional will have various limitations. Thus with one particular DFT functional there couldn't be calculated: good geometries, S_2 ($1^1B_u^+$) state, excitonic splitting and Raman ν_1, ν_2, ν_3 bands. According results it can be concluded that different problemscan be calculatedby choosing different functional only. We didn't compare absolute values between DFT functional result and experimental values which is important also (e.g. B3LYP underestimates S_0-S_2 transitions in Cars).

Comparing different DFT Cars geometries in the work LYC (also other Cars) may have Raman ν_4 bands related possibly to dihedral distortion [37] what could be due to excitonic effect in dimers [37, 45]. The distortion coming from dimers must be analyzed by using the same DFT functional for all type calculations. However, according functional analysis all different properties can be analyses with different functional only.Off course there can be analyzed similar models by ignoring the limitations of the functional but there must be made carefullyinterpretation of the results. The other way is to develop new DFT functional. The new functional should be based on B3LYP

which is good for the monomer calculations but it failson dimer. There is the long range correction in CAM-B3LYP which is good for dimer calculations.

However, the CAM implementations to B3LYP resultsgive worse results for the other calculated properties, such as UV and Raman spectra in monomer.

CONCLUSIONS

There were performed calculations with 281 DFT functional for the TD-DFT of LYC H-dimer and monomer and for Raman ν_1, ν_2, ν_3 bands of LYC monomer. The 255 functional are suitable for the LYC monomer optimization which had results similar to experimental data [37]. TD-DFT analysis for LYC monomer showed there were 92 functional suitable for the modeling S_2 $(1^1B_u^+)$ state.

The 16 functional were suitable for the modeling excitonic splitting with TD-DFT of LYC H-dimer. The 7 functional could be used for the Raman analysis of LYC monomer. However, there wasn't one functional which could have good prediction for all properties: good geometries, S_2 $(1^1B_u^+)$ state, excitonic splitting and Raman ν_1, ν_2, ν_3 bands (Table II).The most promising DFT functional for Cars were B3LYP, CAM-B3LYP and HSEH1PBE. However, in order to model different properties of Cars there should be used different DFT functional.

ACKNOWLEDGEMENTS

REFERENCES

[1] C.-C Huang, Applications of Raman Spectroscopy in Herbal Medicine, App. Spect. Rev. **51** (1), 1-11 (2016).

[2] S. Kumar, N. Matange, S. Umapathy, and S.S. Visweswariah, Linking carbon metabolism to carotenoid production in mycobacteria using Raman spectroscopy, FEMS Microbiol. Lett.**362** (3), 1-6 (2015).

[3] E.Kish, M.M.M. Pinto, D. Kirilovsky, R. Spezia, and B. Robert, Echinenone vibrational properties: From solvents to the orange carotenoid protein, Biochim. Biophys. Acta (BBA) - Bioenergetics **1847** (10), 1044-1054 (2015).

[4] Y.-C Lin, E. Perevedentseva, and C.-L Cheng, Raman spectroscopic study on the excystation process in a single unicellular organism amoeba (Acanthamoeba polyphaga), J Biomed. Opt. **20** (5), 051042 (2015).

[5] J. Garcia-Guinea, M. Furio, S. Sanchez-Moral, V. Jurado, V. Correcher, and C. Saiz-Jimenez, Composition and spectra of copper-carotenoid sediments from a pyrite mine stream in Spain, Spectrochim. Acta A **135**, 203-210 (2015).

[6] E. Kish, K. Wang, M.J. Llansola-Portoles, C. Ilioaia, A.A. Pascal, B. Robert, and C. Yang, Probing the pigment binding sites in LHCII with resonance Raman spectroscopy: The effect of mutations at S123, Biochim. Biophys. Acta (BBA) **1857**, 1490-1496 (2016).

[7] Gall, A.A. Pascal,and B. Robert, Vibrational techniques applied to photosynthesis: Resonance Raman and fluorescence line-narrowing, Biochim. Biophys. Acta (BBA) **1847**, 12-18 (2015).

[8] N. Tonouchi, D. Kosumi, M. Sugisaki, M. Nango, and H. Hashimoto, How do surrounding environments influence the electronic and vibrational properties of spheroidene?, Photosynth. Res.**124**, 77-86 (2015).

[9] Y.S. Tan, D. Urbančok, and R.D. Webster, Contrasting Voltammetric Behavior of Different Forms of Vitamin A in Aprotic Organic Solvents, J. Phys. Chem. B **118**, 8591-8600 (2014).

[10] I.G. Prandi, L. Viani, O. Andreussi, and B. Mennucci, Combining classical molecular dynamics and quantum mechanical methods for the description of electronic excitations: The case of carotenoids, J. Comput. Chem. **37**, 981-991 (2016).

[11] Arteni, M. Fradot, D. Galzerano, M.M. Mendes-Pinto, J. Sahel, S. Picaud, B. Robert, and A.A. Pascal, Structure and Conformation of the Carotenoids in Human Retinal Macular Pigment, PLOS ONE **10**, e0135779 (2015).

[12] L. Fiedor, Heriyanto, J. Fiedor, and M. Pilch, Effects of Molecular Symmetry on the Electronic Transitions in Carotenoids, J. Phys. Chem. Lett. **7**, 1821-1829 (2016).

[13] K. Vijayalakshmi, A. Jha, and J. Dasgupta, Ultrafast Triplet Generation and its Sensitization Drives Efficient Photoisomerization of Tetra- cis -lycopene to All- trans -lycopene , J. Phys. Chem. B **119**, 8669-8678 (2015).

[14] M. Viuda-Martos, E. Sanchez-Zapata, E. Sayas-Barberá, E. Sendra, J.A. Pérez-Álvarez, and J. Fernández-López, Tomato and Tomato

Byproducts. Human Health Benefits of Lycopene and Its Application to Meat Products: A Review, Crit. Rev. Food Sci. Nutr. **54**, 1032-1049 (2014).

[15] P. Singh, G.K. Goyal, Dietary lycopene: Its properties and anticarcinogenic effects, Comp. Rev. Food Sci. Food Safety. **7**, 255–270(2008).

[16] S.K. Clinton, C. Emenhister, S.J. Schwartz, D.G. Bostwick, A.W. Williams, B.J. Moore, J.W. Erdman Jr., Cis-trans lycopene isomers, carotenoids and retinol in the human prostate, Cancer Epidemiol. Biomarkers Prev. **5**, 823-833(1996).

[17] A.L. LeRosen, and C.E. Reid, An Investigation of Certain Solvent Effect in Absorption Spectra, J. Chem. Phys.**20**, 233 (1952).

[18] K. Hirayama, Absorption Spectra and Chemical Structures. I. Conjugated Polyenes and p-Polyphenyls, J. Am. Chem. Soc. **77**, 373-379 (1955).

[19] P.O. Andersson, T. Gillbro, L. Ferguson, and R.J. Cogdell, Absorption Spectral Shifts of Carotenoids Related to Medium Polarizability, Photochem. Photobiol. **54**, 353-360 (1991).

[20] M. Kuici, H. Nagae, R.J. Cogdell, K. Shimada, and Y. Koyama, Solvent Effect on Spheroidene in Nonpolar and Polar Solutions and the Environment of Spheroidene in the Light-Harvesting Complexes of Rhodobacter Sphaeroides 2.4.1 as Revealed by the Energy of the 1ag−→1bu+Absorption and the Frequencies of the Vibronically Coupled C=C Stretching Raman Lines in the 1ag− and 1bu−States, Photochem. Photobiol. **59**, 116-124 (1994).

[21] Z. Chen, C. Lee, T. Lenzer, and K. Oum, Solvent Effects on the S-0(1(1)Ag(-)) → S-2(1(1)B(U)(+)) Transition of Beta-Carotene, Echinenone, Canthaxanthin, and Astaxanthin in Supercritical CO2 And CF3H. J. Phys. Chem. A **110**, 11291-11297 (2006).

[22] Renge, and E. Sild, Absorption shifts in carotenoids—influence of index of refraction and submolecular electric fields, J.Photochem. Photobiol. A **218**, 156-161 (2011).

[23] P. Tavan, and K. Schulten, The low-lying electronic excitations in long polyenes: A PPP-MRD-CI study, J. Chem. Phys. **85**, 6602–6609 (1986).

[24] T. Polívka, and V. Sundström, Dark excited states of carotenoids: Consensus and controversy, Chem. Phys. Lett. **477**, 1-11 (2009).

[25] T. Gillbro, R.J. Cogdell, and V. Sundström, Energy transfer from carotenoid to bacterio chlorophyll a in the B800-820 antenna complexes from Rhodopseudomonas acidophila strain 7050 , FEBS Lett. **235**, 169-172 (1988).

[26] T. Polívka, and V. Sundström, Ultrafast Dynamics of Carotenoid Excited States−From Solution to Natural and Artificial Systems, Chem. Rev. **104**, 2021-2072 (2004).

[27] E. Papagiannakis, J.T.M. Kennis, I.H.M. van Stokkum, R.J. Cogdell, and R. van Grondelle, An alternative carotenoid-to-bacterio chlorophyll energy transfer pathway in photo synthetic light harvesting, P. Natl. Acad. Sci. USA **99**, 6017-6022 (2002).

[28] P. Wang, R. Nakamura, Y. Kanematsu, Y. Koyama, H. Nagae, T. Nishio, H. Hashimoto, and J. Zhang, Low-lying singlet states of carotenoids having 8–13 conjugated double bonds as determined by electronic absorption spectroscopy, Chem. Phys. Lett. **410**, 108-114 (2005).

[29] Y. Koyama, Y. Kakitani, T. Miki, R. Christiana, and H. Nagae, Excited-State Dynamics of Overlapped Optically-Allowed 1Bu+ and Optically-Forbidden 1Bu- or 3Ag- Vibronic Levels of Carotenoids: Possible Roles in the Light-Harvesting Function, IJMS **11**, 1888-1929 (2010).

[30] C.C. Gradinaru, J.T.M. Kennis, E. Papagiannakis, I.H.M. van Stokkum, R.J. Cogdell, G.R. Fleming, R.A. Niederman, and R. van Grondelle, An unusual pathway of excitation energy deactivation in carotenoids: Singlet-to-triplet conversion on an ultrafast timescale in a photosynthetic antenna, PNAS **98**, 2364-2369 (2001).

[31] J. Dale, Empirical Relationships of the Minor Bands in the Absorption Spectra of Polyenes, Acta Chem. Scand.**8**, 1235–1256 (1954).

[32] R. Hemley and , B. Kohler, Electronic Structure of Polyenes Related to the Visual Chromophore. A Simple Model for The Observed Band Shapes. Biophys. J. **20**, 377–382 (1977).

[33] R.L. Christensen, E.A. Barney, R.D. Broene, M.G.I. Galinato, and H.A. Frank, Linear polyenes: models for the spectroscopy and photophysics of carotenoids, Arch. Biochem. Biophys. **430**, 30-36 (2004).

[34] G. Araki, T. Murai, Molecular Structure and Absorption Spectra of Carotenoids, Prog. Theor. Phys. **8**, 639–654 (1952).

[35] H. Suzuki, S. Mizuhuashi, π-Electronic Structure and Absorption Spectra of Carotenoids, J. Phys. Soc. Jpn. **19**, 724–738 (1964).

[36] L. Rimai, R.G. Kilponen, and D. Gill, Excitation profiles of laser Raman spectra in the resonance region of two carotenoid pigments in solution, J. Am. Chem. Soc. **92**, 3824-3825 (1970).

[37] M. Macernis, J. Sulskus, S. Malickaja, B. Robert, L. Valkunas, Resonance Raman Spectra and Electronic Transitions in

Carotenoids: A Density Functional Theory Study, J. Phys. Chem. A **118** 1817-1825 (2014).

[38] S. Saito, and M. Tasumi, Normal-coordinate analysis of retinal isomers and assignments of Raman and infrared bands, J. Raman Spectrosc. **14**, 236-245 (1983).

[39] Wirtz, M. van Hemert, J. Lugtenburg, H. Frank, and E. Groenen, Two Stereoisomers of Spheroidene in the Rhodobacter sphaeroides R26 Reaction Center: A DFT Analysis of Resonance Raman Spectra, Biophys. J.**93**, 981-991 (2007).

[40] E. Kish, M.M. Mendes Pinto, D. Bovi, M. Basire, L. Guidoni, R. Vuilleumier, B. Robert, R. Spezia, and A. Mezzetti, Fermi Resonance as a Tool for Probing Peridinin Environment, J. Phys. Chem. B **118**, 5873-5881 (2014).

[41] M. Macernis, J. Sulskus, C.D.P. Duffy, A.V. Ruban, L. Valkunas, Electronic Spectra of Structurally Deformed Lutein, J. Phys. Chem. A **116,** 9843–9853(2012).

[42] M.J. Frisch, G.W. Trucks, H.B. Schlegel, G.E. Scuseria, M.A. Robb, J.R. Cheeseman, G. Scalmani, V. Barone, B. Mennucci, G.A. Petersson et al. Gaussian 09; Gaussian, Inc.: Wallingford, CT, USA, (2009).

[43] L. Zechmeister, Cis-trans isomerization and stereochemistry of carotenoids and diphenyl-polyenes, Chem. Rev. **34,** 267–344(1944).

[44] J. Koepke, X. Hu, C. Muenke, K. Schulten, H. Michel, The crystal structure of the light-harvesting complex II (B800-850) from Rhodospirillum molischianum, Structure **4**, 581-597(1996).

[45] C.D.P. Duffy, J. Chmeliov, M. Macernis, J. Sulskus, L. Valkunas, A.V. Ruban, Modeling of Fluorescence Quenching by Lutein in the Plant Light-Harvesting Complex LHCII, J. Phys. Chem. B **117**,10974–10986(2013).

[46] Dreuw, P. H. P. Harbach, J. M. Mewes, M. Wormit, Quantum Chemical Excited State

Calculations on Pigment-Protein Complexes Require Thorough Geometry Re-optimization of Experimental Crystal Structures, Theor. Chem. Acc. **125**, 419–426(2010).

[47] Dreuw, M. Head-Gordon, Failure of Time-Dependent Density Functional Theory for Long-Range Charge-Transfer Excited States: The Zincbacteriochlorin−Bacteriochlorin and Bacteriochlorophyll−Spheroidene Complexes, J. Am. Chem. Soc. **126**, 4007–4016(2004).

[48] Y. Koyama, T. Takii, K. Saiki, K. Tsukida, Configuration of theCarotenoid in the Reaction Centers of Photosynthetic Bacteria. 2.Comparison of the Resonance Raman Lines of the Reaction Centerswith Those of the 14 Different Cis−Trans Isomers of Beta-Carotene, Photobiochem. Photobiophys. **5**, 139−150 (1983).

[49] A.V. Ruban,P. Horton, B. Robert, Resonance RamanSpectroscopy of the Photosystem II Light-Harvesting Complex ofGreen Plants: A Comparison of Trimeric and Aggregated States.Biochem. (Moscow) **34**, 2333−2337 (1995).

[50] A.V. Ruban, A.A. Pascal, and B. Robert, Xanthophylls of the major photosynthetic light-harvesting complex of plants: identification, conformation and dynamics, FEBS Lett.**477**, 181-185 (2000).

[51] M.M. Mendes-Pinto, D. Galzerano, A. Telfer, A.A. Pascal, B. Robert, and C. Ilioaia, Mechanisms Underlying Carotenoid Absorption in Oxygenic Photosynthetic Proteins, J. Biol. Chem.**288**, 18758-18765 (2013).

[52] M.W. Wong, Vibrational frequency prediction using Density Functional Theory, Chem. Phys. Lett. **256**, 391–399(1996).

[53] M.Macernis, D. Galzerano, J. Sulskus, E. Kish, Y.H. Kim, S. Koo, L. Valkunas, B. Robert, Resonance Raman spectra of carotenoid molecules: influence of methyl substitutions, J. Phys. Chem. A**119** (1), 56-66 (2014).